*Journal of Sound and Vibration* (2000) **229**(4), 837–857
doi:10.1006/jsvi.1999.2526, available online at http://www.idealibrary.com on IDEAL®

# THE EFFECT OF DETUNING PARAMETERS ON THE ABSORPTION REGION FOR A COUPLED SYSTEM: A NUMERICAL AND EXPERIMENTAL STUDY

OLKAN CUVALCI

*Department of Mechanical Engineering, Texas Tech University, Lubbock, TX* 79409, *U.S.A.*

(*Received* 16 *February* 1999, *and in final form* 6 *July* 1999)

An approach for implementing a passive non-linear vibration controller for flexible structures has been presented. The system consists of introducing the second order controller. When the structure is forced in the neighborhood of its resonance, the controller reduces the structure response. The structure consists of a cantilever beam with a tip mass. A pendulum is attached to the tip mass as a passive vibration controller. The equation of the motion was obtained by assuming that the cantilever beam and the pendulum were subjected to large deflections. In this study, autoparametric interaction was investigated by varying the forcing amplitude, the internal frequency ratio, and the mass ratio in the neighborhood of the autoparametric resonance. The objective of this study was to define an *absorption region* numerically and experimentally with respect to forcing amplitude, internal frequency ratio and mass ratio for the passive vibration absorber.



## 1. INTRODUCTION

A useful technique for the elimination of undesirable vibration of problems of structural dynamics and machinery dynamics has been the application of one or more passive dynamic vibration absorbers. In this study, numerical and experimental applications of a passive vibration absorber for flexible structures are presented. For the numerical simulation, most of the energy is assumed to excite the first mode of the structure. The equation of motion was obtained by assuming that the cantilever beam with a tip mass and the pendulum system is subjected to large deflections, resulting in non-linear coupling between the modes. The absorber is based on the saturation phenomenon of flexible structure exhibited by multi-degree-of-freedom (d.o.f.) systems with quadratic non-linearities possessing two-to-one autoparametric resonances. When the natural frequency of the controller (absorber) is set to one-half of the natural frequency of the structure (resonant mode), the non-linear coupling terms create a unidirectional energy-transfer mechanism that saturates the response of the resonant mode and reduces its vibration [1]. Watts developed the concept of the vibration absorber for the first time in 1883. The first application of a passive vibration absorber was

0022-460X/00/040837 + 21 $35.00/0 

designed by Frahm in 1902 [2]. The application of a vibration absorber to mechanical structures was applied and studied by numerous authors [4–7].

Jacquot [8] developed a technique that gives the optimal dynamic vibration absorber parameters for the elimination of the excessive vibration in sinusoidally forced Bernoulli–Euler beams. Kitis *et al.* [9] investigated an efficient optimal design algorithm for minimizing the vibratory response of a multi-d.o.f. system under sinusoidal excitation over several excitation frequencies. Jordanov and Cheshnakov [10] used the algorithm to obtain optimal parameters for both linearly and non-linearly damped dynamic vibration absorbers. Recently, Dahlberg [11] investigated three types of vibration absorbers: classical single-degree-of-freedom (s.d.o.f.) absorbers, two s.d.o.f. discrete absorbers, and a continuous cantilever beam absorber. The author clearly shows that the continuous vibration absorber is more effective than the other two absorbers. Hitchcock *et al.* [12, 13] investigated a bi-directional liquid column vibration absorber (LCVA) numerically and experimentally for various initial amplitudes of excitation. They also presented techniques that could be used to control the absorber characteristics. In this system, energy dissipation occurs through the viscous interaction between the rigid LCVA container and the LCVA liquid.

A well-tuned vibration absorber reduces the oscillatory energy from the primary structure. This kind of unidirectional energy transfer is well demonstrated in the autoparametric vibration controller. Autoparametric interaction exists when the conditions of internal resonance and external resonance are met simultaneously [14]. The absorber is an internal device, which changes the dynamic response of the original oscillating system between a certain forcing frequency range. The absorber device can be a pendulum, a rotary oscillator, a fluid, a flexible structure, or even a mass–spring system. Autoparametric vibration can also be viewed as a special case of parametric vibration. The basic feature of autoparametric resonance is the energy transfer between the modes. Due to the energy transfer, the lower mode amplitude increases exponentially when the higher mode amplitude decreases. Numerous authors have studied autoparametric resonance [15–18].

Autoparametric vibration absorbers have been studied extensively for structural and machinery systems under sinusoidal and random excitation. Haxton and Barr [19] also studied the autoparametric vibration absorber. He examined a main linear spring mass system under periodic forcing, the motion of which acts parametrically on the motion of an attached absorber system. Bishop *et al.* [20] investigated the parametrically driven pendulum in a large variety of stable periodic and chaotic motions for hanging and inverted equilibrium states. The existence of the periodic and chaotic attractors is verified numerically and experimentally. Queini *et al.* [1] investigated an active non-linear vibration absorber for flexible structures (cantilever beam). The authors assumed a multi-d.o.f. system with quadratic non-linearities that possesses two-to-one autoparametric resonances. They developed the equation of motion with quadratic non-linearities and analyzed the system through perturbation techniques and a numerical simulation. The authors also ran several experiments and compared the results. The autoparametric interaction has also been investigated for dynamical systems under random excitation. Ibrahim *et al.* [21] studied

experimentally and numerically autoparametric interactions of a non-linear 2d.o.f. system in the neighborhood of internal resonance under random excitations. The effects of the system damping ratios, non-linear coupling parameters, internal detuning ratio, and excitation spectral density level were investigated in both studies.

In this paper, a structure, consisting of a cantilever beam with a tip-mass, $m$, and a passive vibration controller, consisting of a pendulum mass, $m$, has been investigated numerically and experimentally. The non-linear equations of motion were developed to investigate the autoparametric interaction between the first two modes of the system. The non-linear terms appear due to large deflections and coupling between the beam and the pendulum. It is assumed that the system involved only the first mode vibration to reduce the partial differential equation (PDF) to an ordinary differential equation (ODE).

In the present study, a series of parametric experimental and numerical studies were performed to investigate the response of the system under sinusoidal excitation. To investigate the non-linear dynamics under autoparametric conditions ($\Omega = \omega_b = 2\omega_p$), the internal frequency ratio was varied between 0·45 and 0·55, the mass ratio varied between 0·08 and 1·0, and the forcing amplitude varied between 0·00125 and 0·0025. The objective of this study was to define an *absorption region* numerically and experimentally with respect to forcing amplitude, internal frequency ratio, and mass ratio for the passive vibration absorber.

## 2. EQUATION OF MOTION

The model consisted of a flexible beam with a tip mass and the pendulum attached to the tip mass by a rod as seen in Figure 1. One end of the beam was clamped to the shaker and a vertical harmonic base excitation, $y_g(t)$, was introduced. The beam width was assumed to be 10 times greater than its thickness. Therefore, the effects of the variations of the shear stresses across a section and the rotary inertia of the beam were neglected. The equation of motion was derived using the Euler–Bernoulli beam theory. This theory defines the bending moment of the beam as

$$M(s) = \frac{EI}{R} = EI\,\frac{v''}{\sqrt{(1 - v'^2)}}. \tag{1}$$

Assuming that $u(\zeta, t)$ and $v(\xi, t)$ describe the displacements in the $x$ and $y$ directions, respectively, then the inextensibility condition of the beam can be written as

$$v'^2 + (1 + u')^2 = 1. \tag{2}$$

Displacement $u$ in the $x$ direction can be defined with respect to displacement $v$ in the $y$ direction as

$$u(\zeta, t) = \zeta - \int_0^{\zeta} \sqrt{(1 - v'^2)}\,\mathrm{d}\eta, \tag{3}$$

where ( $'$ ) denotes differentiation with respect to location $s$.

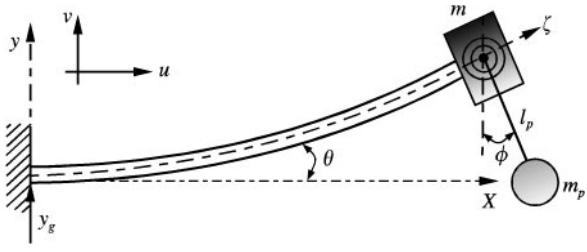


Figure 1. Physical model.

To obtain the equation of motion of the beam with the tip mass, four moment equations can be written at two locations: $\zeta = s$ and $\zeta = L$, in the $x$ and $y$ directions by using D'Alembert's principle. Two of these moment equations are written at $\zeta$ location in the $x$ and $y$ directions, and the other two are written at $\zeta = L$ again in the both directions.

Moment equations at $\zeta$ location in the $x$ and $y$ directions are written as

$$M_{u\zeta} = -\int_s^L \rho A\ddot{u}(\zeta,t)\int_s^\zeta \sin\theta(\zeta,t)\,\mathrm{d}\eta\,\mathrm{d}\zeta \tag{4}$$

and

$$M_{v\zeta} = -\int_s^L [\rho A\ddot{v}(\zeta,t) + c\dot{v}(\zeta,t)]\int_s^\zeta \cos\theta(\zeta,t)\,\mathrm{d}\eta\,\mathrm{d}\zeta, \tag{5}$$

respectively, where $(\cdot)$ represents the time derivative, $\rho A$ is the mass of the beam per unit length and $c$ is the damping of the beam.

Moment equations at $\zeta = L$ location in the $x$ and $y$ directions are written as

$$M_{uL} = \left\{-(m+m_p)\ddot{u}(L,t) + m_p l_p[\ddot{\phi}\cos\phi(L,t) + \dot{\phi}^2\sin\phi(L,t)]\right\}\int_s^L \sin\phi(L,t)\,\mathrm{d}\eta \tag{6}$$

and

$$M_{vL} = \left\{-(m+m_p)\ddot{v}(L,t) + m_p l_p[\ddot{\phi}\sin\phi(L,t) + \dot{\phi}^2\cos\phi(L,t)]\right\}\int_s^L \cos\phi(L,t)\,\mathrm{d}\eta, \tag{7}$$

respectively, where $m$ and $m_p$ are the tip mass and the pendulum mass, respectively, $l_p$ is the length of the pendulum, and $\phi$ is the pendulum angular displacement. The first integrals in equations (4) and (5) and the constant terms in equations (6) and (7) represent the total internal forces acting on the beam, an the second integrals in equations (2) and (3) and the integrals in equations (6) and (7) represent the moment arms. To obtain the beam dynamic equation, equations (1) and (4)–(7) are differentiated twice with respect to location $s$ using Lebniz's rule, and the resulting equations are substituted into the moment balance equation $(M''(s) - M''_{u\zeta} - M''_{v\zeta} - M''_{ul} - M''_{vL} = 0)$. Afterwards, a binomial expansion is

applied to the resulting equation, the terms of order higher than the three are eliminated, and finally, the beam governing equation is obtained as

$$EI\left(v'''' + \frac{1}{2}v'^2 v'''' + v''^3 + v'v''v'''\right) + \rho A v\left[\int_0^\zeta (\dot{v}^2 + v'\ddot{v}')\,\mathrm{d}\eta\right]_{\zeta=s}$$
$$+ v'v''\left[\int_s^L (\rho A\ddot{v} + c\dot{v})\,\mathrm{d}\zeta + \rho A\ddot{y}_g(L-s) + (m+m_p)(\ddot{v}+\ddot{y}_g)\right.$$
$$\left. + m_p l_p(\ddot{\phi}\sin\phi + \dot{\phi}^2\cos\phi)\right]$$
$$- v''\left[\int_s^L \rho A\int_0^\zeta (\dot{v}'^2 + v'\ddot{v}')\,\mathrm{d}\zeta\,\mathrm{d}\eta + (m+m_p)\int_0^\zeta (\dot{v}'^2 + v'\ddot{v}')\,\mathrm{d}\zeta\right.$$
$$\left. - m_p l_p(\ddot{\phi}\cos\phi + \dot{\phi}^2\sin\phi)\right]$$
$$+ \left(1 - \frac{1}{2}v'^2\right)[\rho A(\ddot{v}+\ddot{y}_g) + c\dot{v}] = 0. \tag{8}$$

This equation is non-linear and includes beam terms, coupling (pendulum) terms, and terms of degree no higher than three. It also includes two excitation terms: direct excitation and parametric excitation.

The equation of the pendulum, obtained by equating the total moments with respect to the pivot point of the pendulum to zero, yields

$$\ddot{\phi} + \frac{1}{l_p}(\ddot{v}+g)\sin\phi + \frac{1}{l_p}\ddot{u}\cos\phi + \frac{c_p}{m_p l_p^2}(\dot{\theta}+\dot{\phi}) = 0, \tag{9}$$

where $c_p$ is the damping of the pivot point of pendulum. Equation (9) includes the term $\dot{\theta}$ which needs to be defined in terms of $v$. For this purpose, equation (3) is expended by using binomial expansion and, by eliminating terms of order higher than three, yields

$$\ddot{u} = \int_0^\zeta (\dot{v}'^2 + v'\ddot{v}')\,\mathrm{d}\zeta. \tag{10}$$

Differentiating $v' = \sin\theta$ once with respect to time and expanding the resulting equation using a binomial expansion result in

$$\dot{\theta} = \dot{v}' + \tfrac{1}{2}v'^2\dot{v}', \tag{11}$$

where $\dot{\theta}$ is the angular velocity of the beam. To obtain the final pendulum equation substituting equations (10) and (11) into equation (9) gives

$$\ddot{\phi} + \frac{1}{l_p}(\ddot{v}+\ddot{y}_g+g)\sin\phi + \frac{1}{l_p}\int_0^\zeta (\dot{v}'^2 + v'\ddot{v}')\,\mathrm{d}\zeta\cos\phi + \frac{c_p}{m_p l_p^2}\left(\dot{v}' + \frac{1}{2}v'^2\dot{v}' + \dot{\phi}\right) = 0. \tag{12}$$

The pendulum equation includes non-linear terms, coupling terms, and a parametric excitation term.

Equations (8) and (12) are two coupled non-linear equations which characterize the dynamics of the beam-tip mass–pendulum system. The system of equations does not have closed-form solutions. The model was governed by a set of partial differential equations which involve infinite model series. The Galerkin method is used to obtain a set of ODEs from the given PDEs for an approximate solution. In this study, it is assumed that the first mode of the system is dominant, therefore, the truncated displacement function becomes

$$v(s,t) = ry(s)z(t), \tag{13}$$

where $r$ is a scaling factor, $y(s)$ is a set of orthonormal functions (usually a solution of the linear equation of the system), and $z(t)$ is an unknown time modulation of the linear problem or mode. Substituting equation (13) into equations (8) and (12) the orthogonalizing the error with respect to the eigenfunction, the following ordinary differential equations are obtained for the beam and the pendulum, respectively:

$$\ddot{z} = -[G_3 c\dot{z} + G_4 c\dot{z}z^2 + G_5 \dot{z}^2 z + (G_6 + t_{13}\ddot{\phi}\cos\phi + t_{14}\dot{\phi}^2 \sin\phi)z + (G_7 \ddot{y}_g + t_{17}\ddot{\phi}\sin\phi + t_{18}\dot{\phi}^2\cos\phi)z^2 + G_8 z^3 + G_9 \ddot{y}_g]/(G_1 + G_2 z^2)$$

and

$$\ddot{\phi} = -\left[\frac{1}{l_p}(P_4\ddot{z} + \ddot{y}_g + g)\sin\phi + \frac{P_1}{l_p}(\dot{z}^2 + z\ddot{z})\cos\phi + \frac{c_p}{m_p l_p^2}\left(P_2\dot{z} + \frac{1}{2}P_3\dot{z}z^2 + \dot{\phi}\right)\right], \tag{14}$$

where $G_1, \ldots, G_9$ and $P_1, \ldots, P_4$ are the Galerkin coefficients of the beam and the pendulum, respectively [22]. Equation (14) includes the first mode terms of the beam-tip mass-pendulum system and is ready for the numerical analysis.

## 3. EXPERIMENTAL SYSTEM

The experimental set-up is shown in Figure 2. The primary structure (cantilever beam), which was 336 mm long, 1·56 mm thick, and 25·4 mm wide with a 0·212 kg tip mass, was mounted at one end of the shaker. The absorber (pendulum) is attached to the encoder which is mounted into the tip mass. The sinusoidal excitation is introduced vertically to the one end of the cantilever beam via a rigid attachment.

A vibration control system consisting of a sweep generator (Trig-Tek Model 701 LM), a signal compressor (Trig-Tek model 801 B), a vibration monitor (Trig-Tek Model 610 B), and a multi-level programmer (Trig-Tek Model 831) is used to generate the sinusoidal excitation signal. A power amplifier (MB Dynamic Model S6K) is used to amplify the generated signal. The signal drives a 1200 lb electrodynamic shaker (MB Dynamics Model C10E). The data acquisition system consists of an Apple Macintosh IIfx computer with a National Instruments NB-MIO-16X board and a Lab View 3.1 analysis and data acquisition software. Additionally, a four-channel digital storage and analysis system (Data 6000) is used.

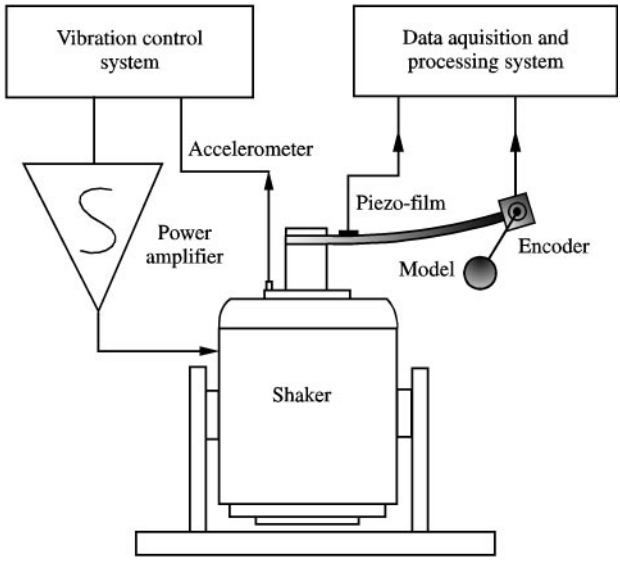


Figure 2. Model with experimental system.

The sinusoidal signal generators also have feedback signals from the shaker to accomplish the task of signal control.

The shaker system is capable of providing different excitation amplitudes and excitation frequencies. The excitation frequency can be swept up and down, with a frequency increment of 0·1 oct/min, in the chosen frequency range by the vibration control system. The Opto-digital encoder was mounted into the tip mass in order to measure the relative angular motion between the tip mass and the pendulum. An accelerometer sends a feedback signal to the vibration control system to control the output of the shaker. A piezo-film is used to detect the strain on the cantilever beam.

## 4. RESULTS AND DISCUSSIONS

To observe the dynamics of the system, three different groups of plots were performed numerically and experimentally. The first group indicates that the beam and the pendulum response is a function of forcing frequency. These plots include data obtained by sweeping the range between two forcing frequencies where the natural frequency of the beam lies. The plots were produced in two ways (up and down sweeps) and a constant sweep rate was used for both. Therefore, the border of the autoparametric region (absorption region) was observed from these two sweeps. This frequency sweep approach is similar to that used by Mustafa and Erats [23] to study a column-pendulum oscillator. For the current study, the forcing frequency increment (sweep rate) is taken to be 0·0015 Hz for the numerical integration and 0·1 oct/min for the experimental analysis. The sweep rate is taken to be small enough for the system to reach steady state at each forcing frequency increment. The experimental sweep rate is the smallest rate available from the control system.

The results were plotted as the numerical and experimental frequency response curves that include data points of local maximums of each period. The arrows on the plots show the sweep direction.

If the response of the beam or the pendulum is $n$ periodic, there should be $n$ local maximums in one period [24]. In the numerical and the experimental results, one or two patterns ($n = 1$ or 2) were observed between the two forcing frequencies. In other words, the system is strongly periodic because direct excitation is dominant in the system. There are portions that include scattered points in the figures. However, the motion is also periodic with $n$-periods in these portions.

The second group of plots shows the effect of different mass ratios ($m_p/m$) and forcing amplitudes on the absorption region. For this analysis, the internal frequency ratio ($\omega_p/\omega_b = 0{\cdot}5$), the natural frequency ($\omega_b = 3{\cdot}07$ Hz), and the forcing amplitude are taken to be constant during both numerical and experimental analyses. The plots include data points that refer to the first jump frequencies of the pendulum or the beam during the up and down sweeps.

The third group of plots shows the effect of forcing amplitude on the absorption and non-absorption regions. For this analysis, the mass ratio ($m_p/m = 0{\cdot}125$), the internal frequency ratio ($\omega_p/\omega_b = 0{\cdot}5$), and the natural frequency ($\omega_b = 3{\cdot}07$ Hz)

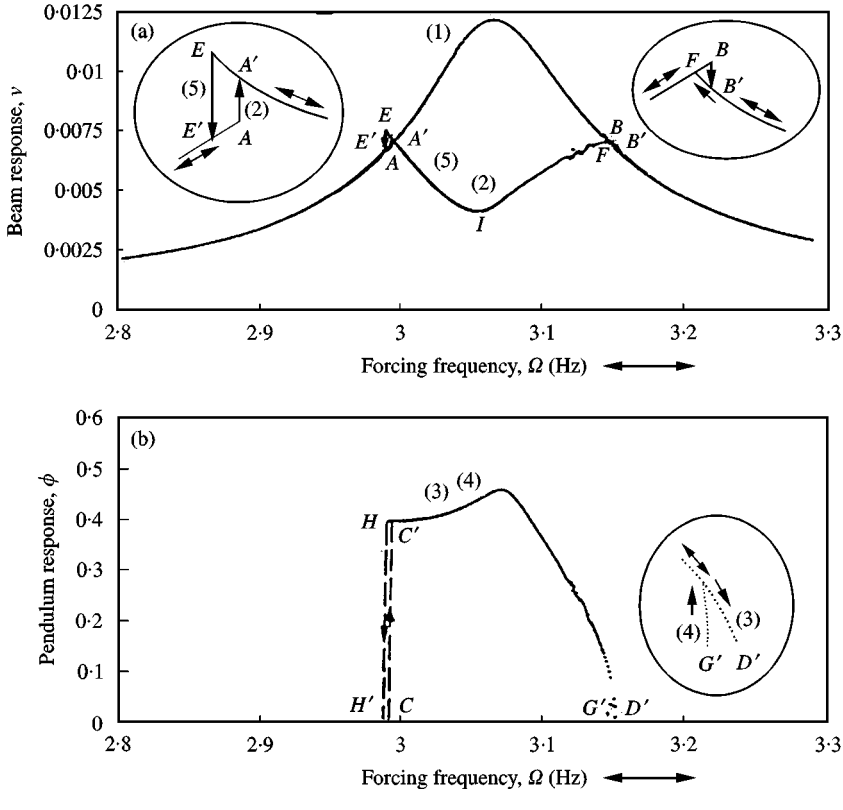


Figure 3. Numerical frequency response curves of $\omega_p/\omega_b = 0{\cdot}5$ for up and down sweeps: (a) beam; (b) pendulum. Response with locked pendulum: (1) beam. Responses with unlocked pendulum. Up sweep: (2) beam; (3) pendulum. Down sweep: (5) beam; (4) pendulum. A, A′, B, B′, C, C′, D′, E, E′, G′, H and H′ jump points for up and down sweeps.

are taken to be constant for both analyses. The plots include numerical and experimental data points that refer to the first and the second jump frequencies of the pendulum and the beam during the up and down sweeps.

### 4.1. NUMERICAL RESULTS

The DIVPAG of the IMSL routine was used for the numerical integration. The results of the integration are presented for the following system parameters: $\rho A = 0{\cdot}31683312$ kg/m, $m = 0{\cdot}212$ kg, $L = 0{\cdot}336$ m, $I = 8{\cdot}669867\text{E-}12$ m$^4$. The system parameters are varied such that, the range of the internal frequency ratio $\omega_p/\omega_b = 0{\cdot}47$–$0{\cdot}53$, the mass ratio $m_p/m = 0{\cdot}01$–$1{\cdot}0$, and the forcing amplitude $f = 0{\cdot}00125$ and $0{\cdot}0025$ m. During the numerical integration, the time increment $\mathrm{d}t = 0{\cdot}01$ s, and the sweep rate increment of $0{\cdot}0015$ Hz are taken to be constant. The natural frequency of the structure with the absorber locked comes out to be $\omega_b = 3{\cdot}07$ Hz.

Figure 3 shows the analytically obtained, four distinct frequency response curves for the cantilever beam and the pendulum. The first and the second curves are obtained with the absorber locked for up and down sweeps while the third and

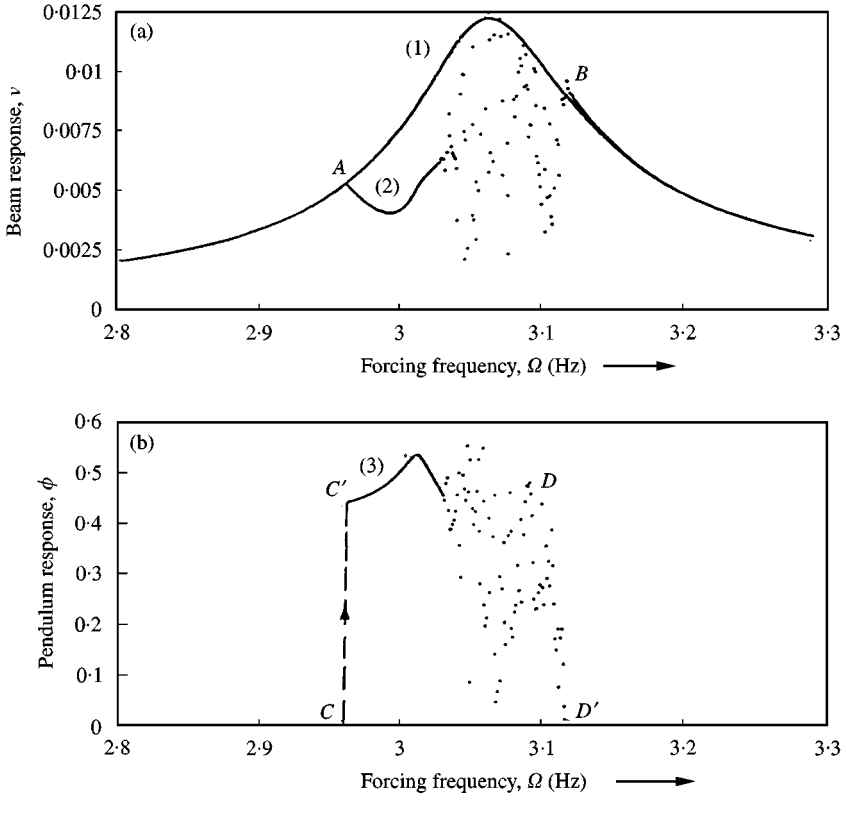


Figure 4. Numerical frequency response curves of $\omega_p/\omega_b = 0{\cdot}475$ for up sweep: (a) beam; (b) pendulum. Response with locked pendulum: (1) beam. Responses with unlocked pendulum: (2) beam; (3) pendulum. A, B, C, C′, D and D′ jump points.

fourth curves were obtained with the absorber activated for both of the sweeps. Curve 1 represents the characteristic response of the absorber locked for both of the sweeps, while Curve 2 (data along AA′IBB′) represents the characteristic response of the cantilever beam with the tip mass for the sweep. Curve 5 (data along FIEE′) shows the characteristic response of the cantilever beam with the tip mass for the down sweep. Curve 3 (data along CC′D′) shows the characteristic response of the absorber for the up sweep. Curve 4 (data along G′HH′) represents the characteristic response of the absorber for the down sweep. In this figure, Curves 3 and 4 correspond to Curves 2 and 5, respectively. The cantilever beam response, Curves (1, 5 and 2), and the controller response, Curves (3 and 4), are obtained to show the unidirectional energy transfer between the modes.

In Figure 3, the internal frequency ($\omega_p/\omega_b = 0{\cdot}5$), mass ratio ($m_p/m = 0{\cdot}125$), and forcing amplitude ($f = 0{\cdot}00125$ m) were taken to be constant to obtain Curves (1–5) with and without the vibration absorber. These curves clearly show that the controller effectively reduces the peak amplitude of the cantilever beam (primary structure). On these curves, the jump phenomenon was observed such as AA′ for the cantilever beam and CC′ for the pendulum during the up sweep and EE′ for the beam and HH′ for the pendulum during the down sweep. These responses are

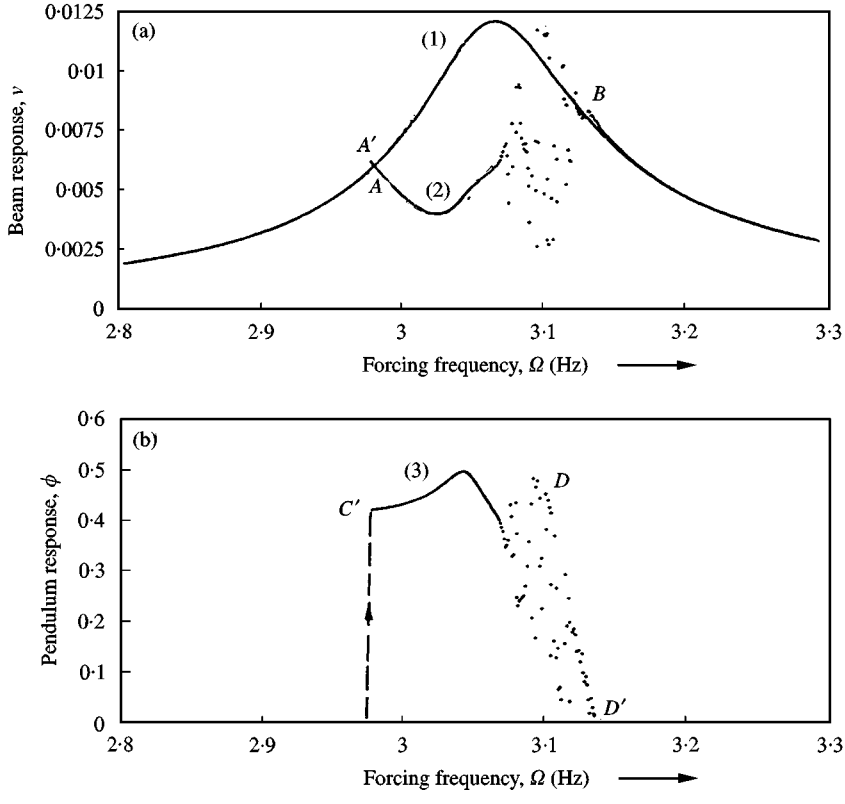


Figure 5. Numerical frequency response curves of $\omega_p/\omega_b = 0{\cdot}49$ for up sweep: (a) beam; (b) pendulum. Response with locked pendulum: (1) beam. Responses with unlocked pendulum: (2) beam; (3) pendulum. Jump points A, A′ B, C, C′, D and D′.

similar to those obtained by other authors studying the effectiveness of different vibration absorbers [11, 19, 24, 25]. From this figure, it is evident that point A for the cantilever beam and point C for the absorber indicate the *starting points* of the interaction between the modes during the up sweep. Point F for the cantilever beam and point G′ for the absorber indicate the starting points of the interaction between the modes during the down sweep. The region between starting points, A and F or C and G′, is called the absorption region. This type of energy interaction has been observed by other researchers while investigating non-linear coupled oscillators [25–28]. From Figure 3, it is also evident that within the absorption region the amplitude of the primary structure is lower when the absorber is used. In this region, the minimum response of the primary structure as observed at the point which satisfied the autoparametric conditions ($\Omega = \omega_b = 2\omega_p$). It is important to note that when comparing Curve 2, between points F and B′, and Curve 5, between the points A′ and E, the energy transfer occurs from the controller to the primary structure. Therefore, the regions between points A′ and E, and F and B′ and called the non-absorption region.

Figures 4, 5, 6, 7 and 8 show frequency response curves of the cantilever beam (with and without the absorber) and the controller for internal detuning ratios of

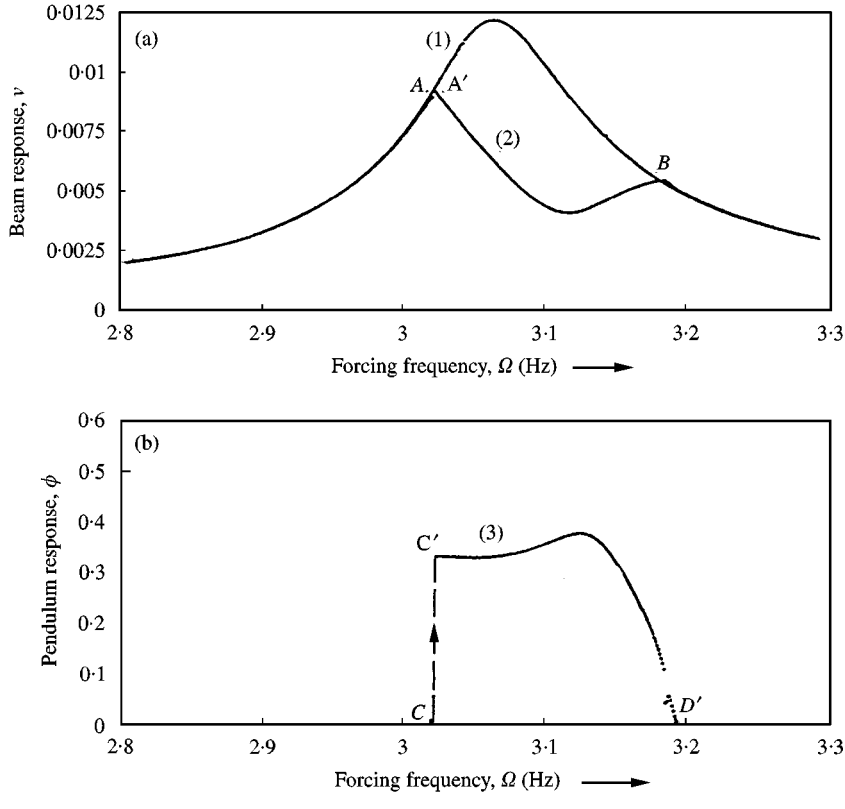


Figure 6. Numerical frequency response curves of $\omega_p/\omega_b = 0{\cdot}51$ for up sweep: (a) beam; (b) pendulum. Response with locked pendulum: (1) beam. Responses with unlocked pendulum: (2) beam; (3) pendulum. A, A′ B, C, C′, and D′ jump points.

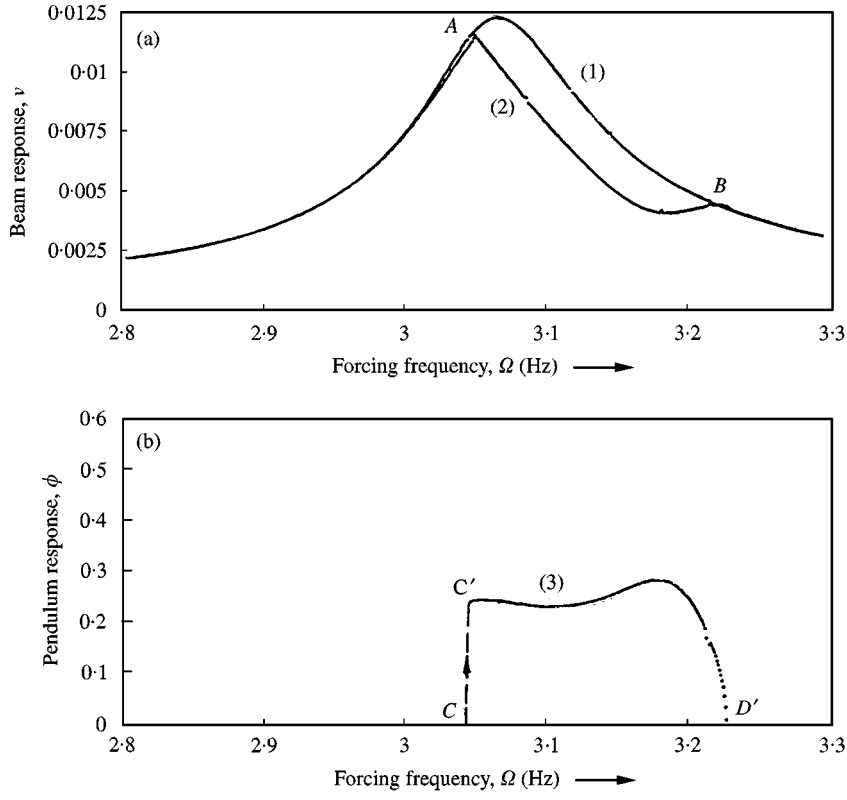


Figure 7. Numerical frequency response curves of $\omega_p/\omega_b = 0{\cdot}525$ for up sweep: (a) beam; (b) pendulum. Response with locked pendulum: (1) beam. Responses with unlocked pendulum: (2) beam; (3) pendulum. A, B, C, C′, and D′ jump points.

0·475, 0·49, 0·51, 0·525 and 0·53 respectively. The internal detuning ratio is defined as $\Delta = \omega_p/\omega_b$. As shown in Figure 4, where $\Delta = 0{\cdot}475$, the autoparametric interaction occurs at 2·92 Hz; and in Figure 5, where $\Delta = 0{\cdot}49$, the same interaction occurs at 3·01 Hz, which are both less than the resonance frequency of 3·07 Hz. On the other hand, in Figure 6, where $\Delta = 0{\cdot}51$, the autoparametric interaction occurred at 3·13 Hz; and in Figure 7, where $\Delta = 0{\cdot}51$, the same interaction occurred at 3·21 Hz, which are both greater than the resonance frequency of 3·07 Hz. From these figures, it is clear that if the internal detuning ratio is lower or higher than 0·5, there is no significant unidirectional energy transfer between the modes. The internal detuning ratio should be 0·5 for the maximum energy interaction between the modes; then the beneficial effect of the controller persists with the very sensitive internal detuning ratio.

In Figure 8, where $\Delta = 0{\cdot}53$, the autoparametric interaction occurs at 3·254 Hz, which is greater than the resonance frequency of 3·07 Hz. For this ratio, the energy interaction cannot be observed because of the high internal detuning ratio. In other words, the high detuning ratio disrupts the coupling between the cantilever beam and the pendulum. Therefore, both the beam and the pendulum behave like two different s.d.o.f. systems.

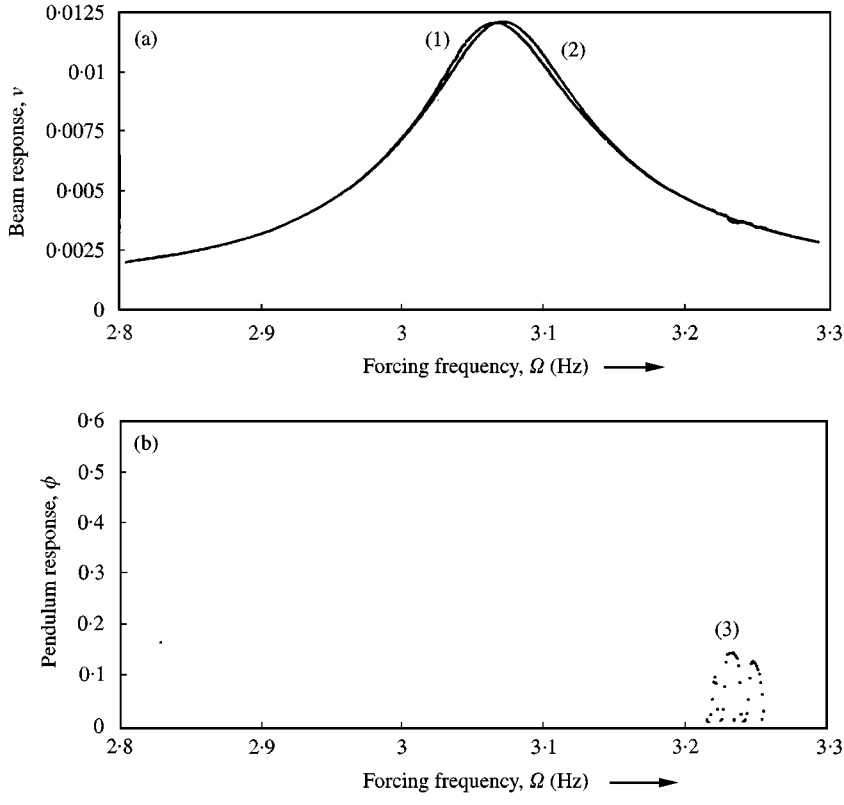


Figure 8. Numerical frequency response curves of $\omega_p/\omega_b = 0{\cdot}53$ for up sweep: (a) beam; (b) pendulum. Response with locked pendulum: (1) beam. Responses with unlocked pendulum: (2) beam; (3) pendulum.

### 4.2. EXPERIMENTAL RESULTS

The same system of parameters (the internal frequency, $\omega_p/\omega_b = 0{\cdot}5$, the mass ratio, $m_p/m = 0{\cdot}125$, and the forcing amplitude, $f = 0{\cdot}00125$ m) used in the numerical analysis were used for the experiments as well. Figure 9 has the same definition as Figure 3 with the difference of being observed experimentally. The variables continue to represent the same curves as well as representing the same up and down sweeps. In this study, it is evident that point A for the cantilever beam and point C for the absorber indicate the *starting points* of the interaction between the modes during the up sweep. Point F for the cantilever beam and point G′ for the absorber indicate the *starting points* of the interaction between the modes during the down sweep. The region between starting points, A and F or C and G′, is again called the *absorption region* during the energy interaction between the modes. This type of energy transfer and the similar responses have been observed by other researchers while investigating autoparametric coupled systems [6, 10, 12, 22]. From Figure 9, the region between points A′ and E as well as F and B′ is the *non-absorption region* as defined previously.

Figure 10, 11, 12 and 13 show the frequency response curve of the cantilever beam (with and without the absorber) and the controller for the internal detuning

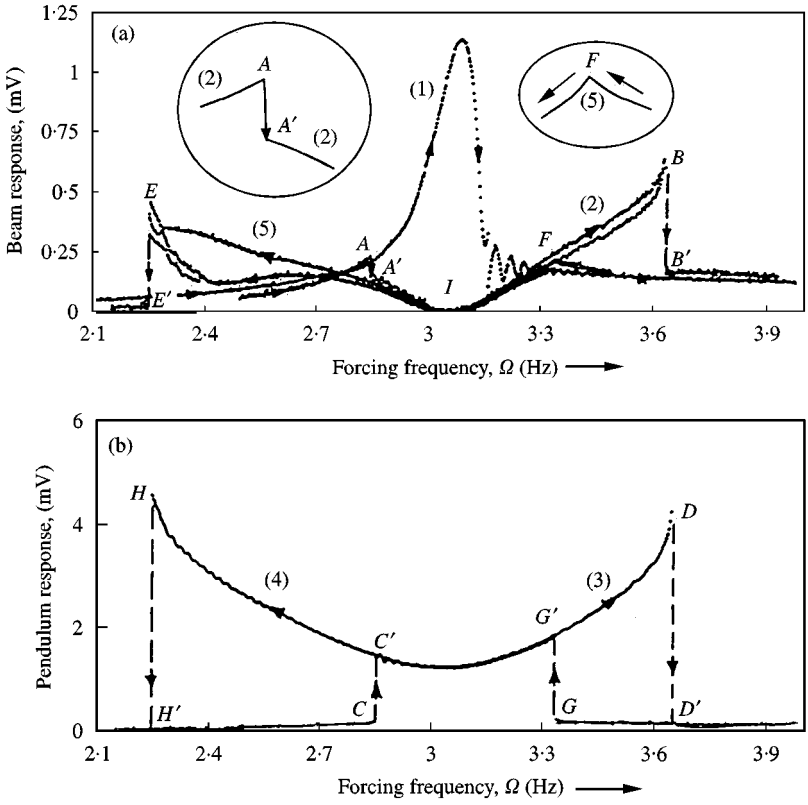


Figure 9. Experimental frequency response curves of $\omega_p/\omega_b = 0{\cdot}5$ for up and down sweeps: (a) beam; (b) pendulum. Response with locked pendulum: (1) beam. Responses with unlocked pendulum. Up sweep: (2) beam; (3) pendulum. Down sweep: (4) pendulum; (5) beam. A, A′, B, B′, C, C′, D, D′ E, E′, F, G, G′, H and H′ jump points for up and down sweeps.

ratios of 0·45, 0·47, 0·53 and 0·55, respectively. As seen in Figure 10, where $\Delta = 0{\cdot}45$, the autoparametric interaction occurs at 2·76 Hz and in Figure 5, where $\Delta = 0{\cdot}47$, the same interaction occurred at 2·95 Hz. Both frequencies are less than the resonance frequency of 3·07 Hz. On the other hand, in Figure 6, where $\Delta = 0{\cdot}53$, the autoparametric interaction occurs at 3·25 Hz; and in Figure 7, where $\Delta = 0{\cdot}55$, the same interaction occurs at 3·34 Hz. Both frequencies are greater than the resonance frequency of 3·07 Hz. From these figures, it is also clear that if the internal detuning ratio is less or greater than the ratio of 0·5, there is no significant unidirectional energy transfer between the modes. The experiments show that the internal detuning ratio should be 0·5 for the maximum energy interaction between the modes. Cuvalci *et al.* [25] performed similar types of experiments for a one-storey building with a continuous absorber. They observed the same kind of dynamic phenomenon.

### 4.3. COMPARISON

Figure 14(a) shows numerically and Figure 14(b) shows experimentally the variations of the absorption region with respect to the mass ratio as well as the

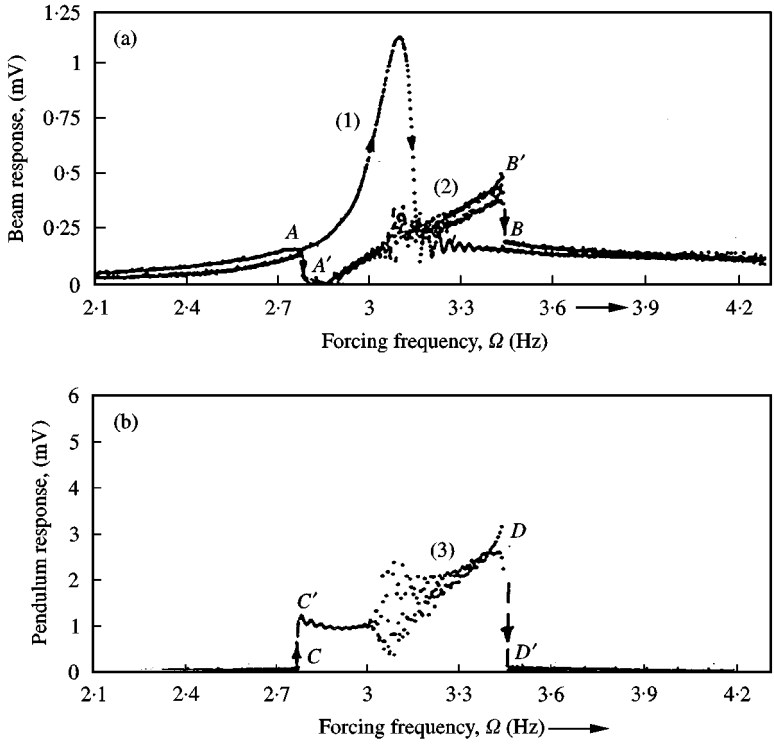


Figure 10. Experimental frequency response curves of $\omega_p/\omega_b = 0{\cdot}45$ for up sweep: (a) beam; (b) pendulum. Response with locked pendulum: (1) beam. Responses with unlocked pendulum: (2) beam; (3) pendulum. A, A′, B, B′, C, C′, D, and D′ jump points.

forcing amplitude. To obtain these figures, the natural frequency of the beam (3·07 Hz), the internal detuning ratio (0·5), and the forcing amplitudes (0·00125 and 0·0025 m) were taken to be constant, and the mass ratio is varied from 0·05 to 1·0. For different mass ratios, frequency response curves are obtained experimentally and numerically (Figures 3 and 9). In these figures, points A and F are used to construct Curves 1 and 2 respectively. Curves 1 and 2 in these figures show the variations of the first jump points with respect to mass ratio during up and down sweeps. From the figures, it is observed that the mass ratio has no effect on the absorption region at a constant forcing amplitude if the absorber mass is greater than 20% of the main mass (mass ratio = 0·2). In other words, a mass ratio of 0·2 provides large ranges of the absorption region. However, if the mass ratio is in between 0·1 and 0·2, there is no noticeable change in the absorption region. In addition, if the mass ratio is less than 0·05, the absorption region becomes very narrow. Therefore, if the absorber mass is in between 5 and 10% of the main mass, a sufficiently wide absorption region in the neighborhood of the autoparameteric region is created. Dahlberg [11] also used 5% of the main mass as the absorber mass to investigate the effectiveness of three different dynamic vibration absorbers. In this study, additional experimental and numerical analyses were performed by varying the forcing amplitude to show the range of the absorption region. The higher forcing amplitudes create wider absorption regions.

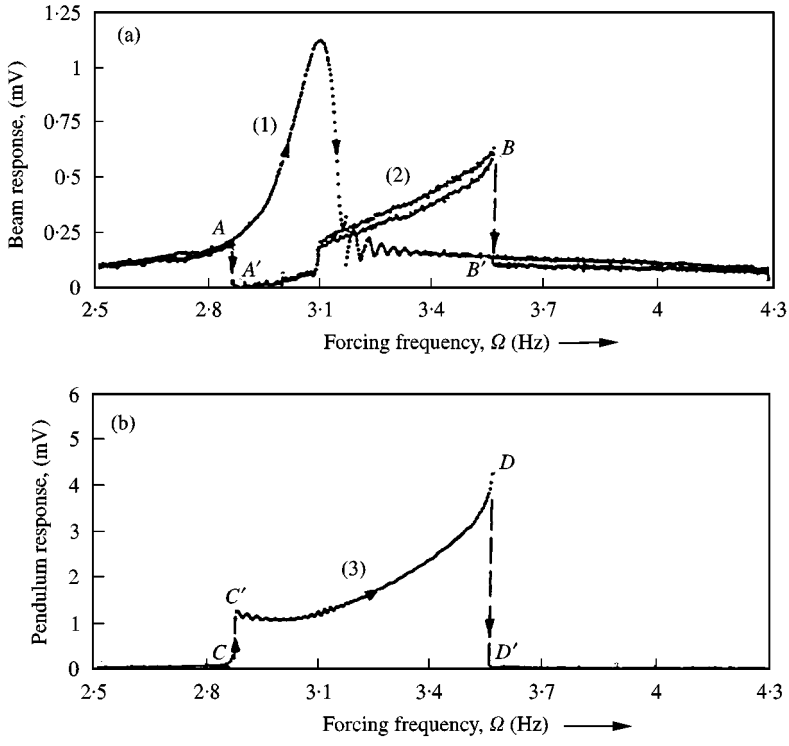


Figure 11. Experimental frequency response curves of $\omega_p/\omega_b = 0{\cdot}47$ for up sweep: (a) beam; (b) pendulum. Response with locked pendulum: (1) beam. Responses with unlocked pendulum: (2) beam; (3) pendulum. A, A′, B, B′, C, C′, D, and D′ jump points.

Figure 15(a) shows numerically and Figure 15(b) shows experimentally the variations of the absorption region and the non-absorption region with the forcing amplitude. To obtain these figures, the mass ratio (0·125), the natural frequency of the beam (3·07 Hz), and the internal frequency ratio (0·5) were taken to be constant, and the forcing amplitude was varied from 0·0005 to 0·003 m for the experiments. Again, frequency response curves are obtained experimentally and numerically (Figures 3 and 9) for different forcing amplitudes. From these figures, points E, A, F and B are are used to construct Curves 3, 1, 2 and 4, respectively. In these figures, Curves 1 and 4 show the variation of the first and the second jump points with the forcing amplitude during the up sweep. Curves 2 and 3 show the variation of the first and second jump points with the forcing amplitude during the down sweep. From these figures, it is observed that both regions vary with the forcing amplitude, and higher forcing amplitudes provide larger absorption regions in both cases [25].

Figure 16 shows numerically the response of the beam (Figure 16(a)) and the pendulum (Figure 16(b)) at the resonance frequency with respect to internal frequency ratio and Figure 17 shows experimentally the response of the beam (Figure 17(a)) and the pendulum (Figure 17(b)) at the resonance frequency with respect to internal frequency ratio. The values of the response of the beam and pendulum at the resonance frequency from the frequency response curves (for example, Figures 3 and 9) are constructed to obtain Figures 16 and 17. These

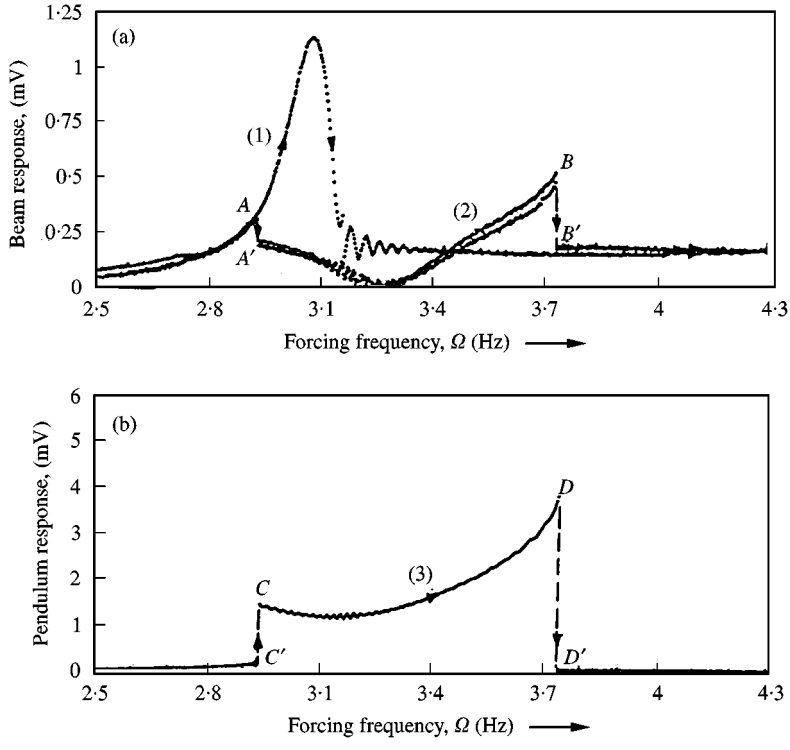


Figure 12. Experimental frequency response curves of $\omega_p/\omega_b = 0{\cdot}53$ for up sweep: (a) beam; (b) pendulum. Response with locked pendulum: (1) beam. Responses with unlocked pendulum: (2) beam; (3) pendulum. A, A′, B, B′, C, C′, D, and D′ jump points.

figures clearly show that maximum energy transfer occurs at the internal frequency ratio of 0·5. At this point, the beam response is a minimum while the pendulum response is at its maximum. When the internal frequency ratio deviates from 0·5, the beam response increases while the pendulum response decreases. When the internal frequency ratio is greater than 0·53 or less than 0·475, the coupling between the beam and the pendulum cannot be observed. At those internal frequency ratios, the pendulum still oscillates, but it does not absorb energy from the beam. In the experimental analysis, the same dynamic behaviors were observed with the numerical analysis. However, the system does not become stable when the internal frequency ratio is set lower than 0·4 or greater than 0·6. Therefore, the experiments could not be performed at these ratios. Moreover, the experimental results show wider absorption regions than the ones obtained with the numerical analysis.

## 5. CONCLUSIONS

The basic absorption action of the autoparametric system under sinusoidal excitation was comprehensively investigated numerically and experimentally. This study involves defining an absorption region for the absorber depending on the

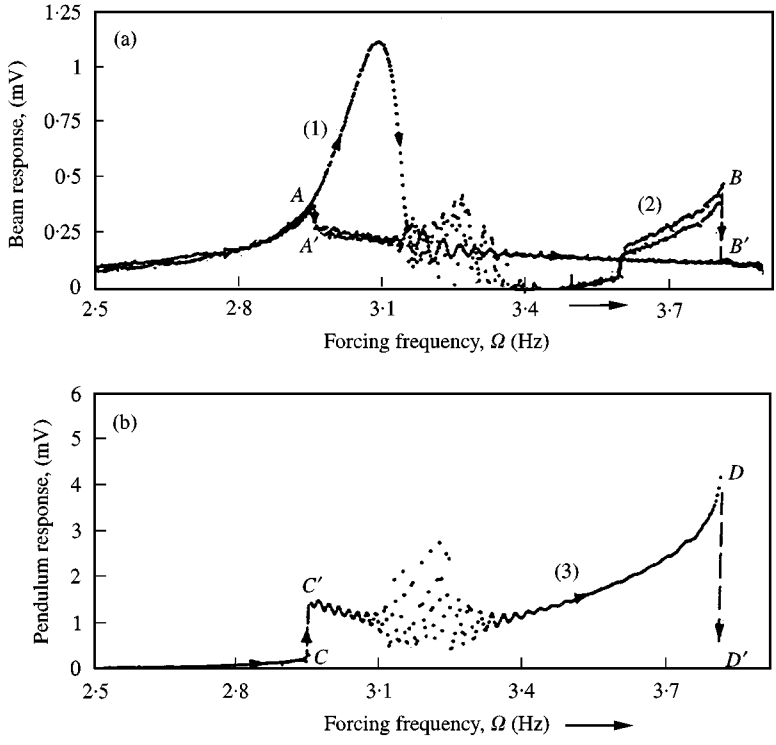


Figure 13. Experimental frequency response curves of $\omega_p/\omega_b = 0{\cdot}55$ for up sweep: (a) beam; (b) pendulum. Response with locked pendulum: (1) beam. Responses with unlocked pendulum: (2) beam; (3) pendulum. A, A′, B, B′, C, C′, D, and D′ jump points.

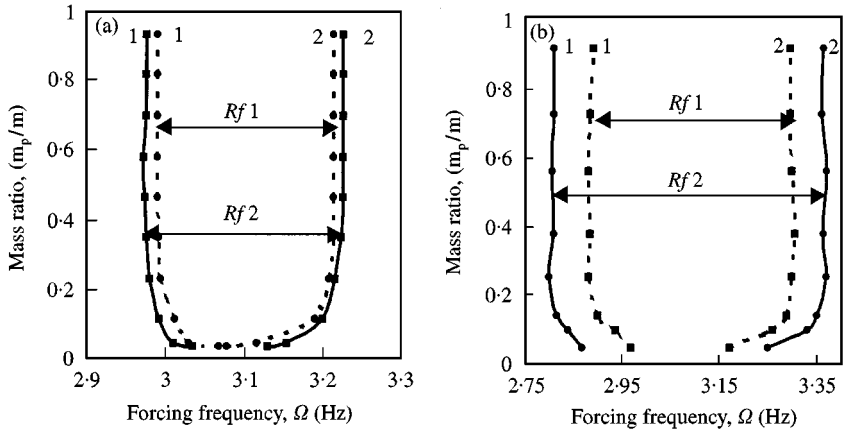


Figure 14. Variation of absorption region with respect to mass ratio at the constant internal frequency ratio ($\omega_p/\omega_b = 0{\cdot}5$): (a) numerical; (b) experimental. Rf1, absorption region for $f = 150$ mV between the lines 1 and 2 (- - -). Rf2, absorption region for $f = 300$ mV between the lines 1 and 2 (——).

control parameters, which are the internal detuning ratio, the mass ratio, and the forcing amplitude. Consequently, the effects of these parameters on the absorption region were established by conducting up and down sweeps. The experimental and

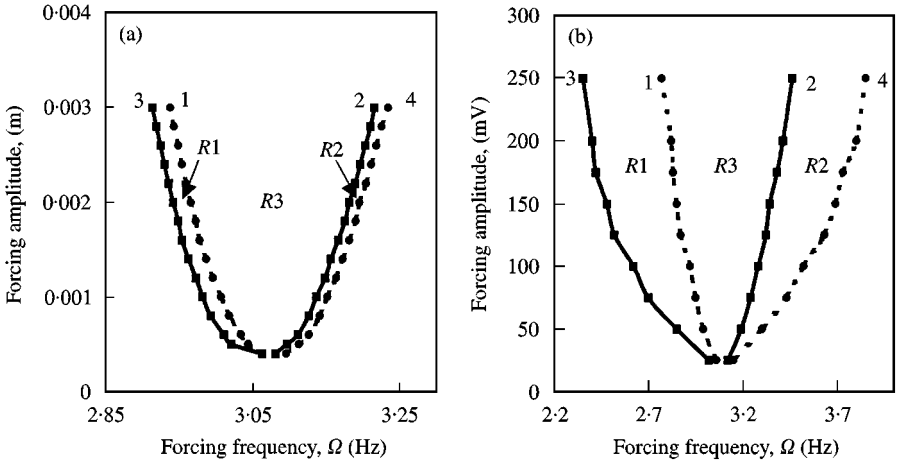


Figure 15. Variation of absorption and nonabsorption regions with respect to forcing amplitude at the constant internal frequency and mass ratios ($\omega_p/\omega_b = 0{\cdot}5$ and $m_p/m = 0{\cdot}125$): (a) numerical; (b) experimental. R1 and R2, non-absorption regions between the lines 1 and 3 as well as 2 and 4. R3, absorption region between lines 1 and 2.

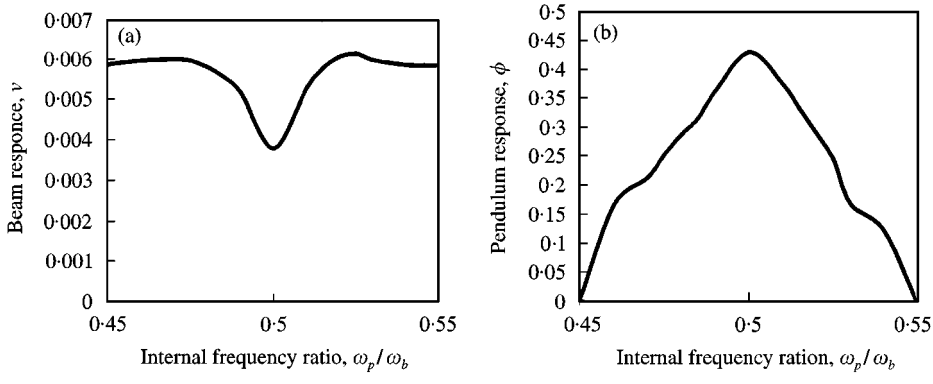


Figure 16. Numerical response at the resonance frequency with respect to internal frequency ratio: (a) beam, (b) pendulum.

numerical results show that the beneficial unidirectional energy transfer appears between the cantilever beam with the tip mass and the absorber when the autoparametric condition, $\Omega = \omega_b = 2\omega_p$, is satisfied. However, the effect of the absorber on the absorption region is proportional to the internal detuning ratio. When the detuning ratio deviates from 0·5 ($\omega_p/\omega_b < 0{\cdot}5 < \omega_p/\omega_b$), the unidirectional energy transfer between the modes cannot be observed. Therefore, the beneficial effect of the controller is depending on a sensitive internal detuning ratio. Moreover, both studies show that the higher forcing amplitudes result in larger absorption regions. It is also observed that the beneficial absorber effect resulting from increasing mass ratio, ceased when it is lower than 0·05 or higher than 0·10.

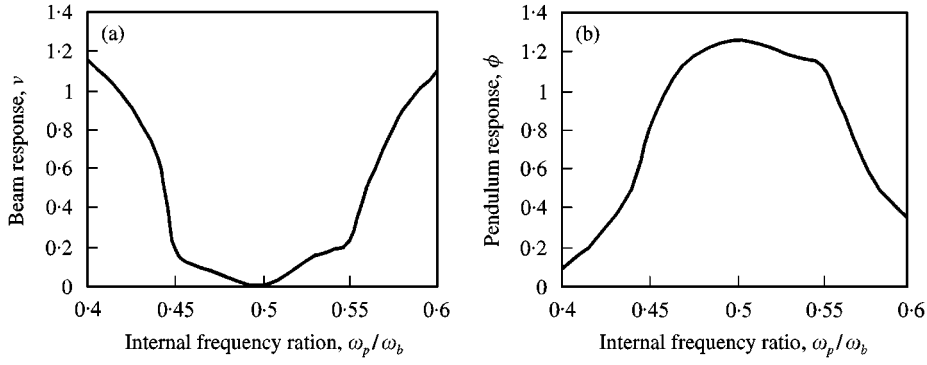


Figure 17. Experimental response at the resonance frequency with respect to internal frequency ratio: (a) beam, (b) pendulum.

## REFERENCES


1. S. S. Oueini, A. H. Nayfeh and J. R. Pratt 1998 *Nonlinear Dynamics* **15**, 259–282. A nonlinear vibration absorber for flexible structures.
2. J. P. Den Hartog 1985 *Mechanical Vibration* New York.
3. P. Watts 1883 *Transactions of International of Naval Architects* **24**, 90–165. On a method of reducing the rolling of ships at sea.
4. A. H. Nayfeh and L. D. Zavodney 1986 *Journal of Sound and Vibration* **107**, 329–350. The response of two-degree-of-freedom system with quadratic non-linearities to a combination parametric resonance.
5. R. G. Mitchiner and R. G. Leonard 1991 *Journal of Vibration and Acoustics* **113**, 503–507. Centrifugal pendulum vibration absorbers—theory and practice.
6. M. F. Golnaraghi 1991 *Journal of Mechanics Research Communications* **18**, 135–143. Vibration suppression of flexible structures using internal resonance.
7. C-.T. Lee and S. W. Shaw 1996 *Journal of Sound and Vibration* **191**, 695–719. On the counteraction of periodic torque for rotating system using centrifugal driven vibration absorber.
8. R. G. Jacquot 1978 *Journal of Sound and Vibration* **60**, 535–542. Optimal vibration absorbers for general beam system.
9. L. Kitis 1983 *Journal of Sound and Vibration* **89**, 559–569. Vibration reduction over a frequency range.
10. I. N. Jordanov and B. I. Cheshankov 1988 *Journal of Sound and Vibration* **123**, 157–170. Optimal design of linear and non-linear dynamic vibration absorbers.
11. T. Dahlberg 1989 *Journal of Sound and Vibration* **132**, 518–522. On optimal use of the mass of a dynamic vibration absorber.
12. P. A. Hitchcock, K. C. S. Kwok, R. D. Watkins and B. Samali 1997 *Engineering Structures* **19**, 126–134. Characteristics of liquid column vibration absorbers (LCVA)—I.
13. P. A. Hitchcock, K. C. S. Kwok, R. D. Watkins and B. Samali 1997 *Engineering Structures* **19**, 135–144. Characteristics of liquid column vibration absorbers (LCVA)—II.
14. R. A. Ibrahim and A. D. S. Barr 1975 *Journal of Sound and Vibration* **42**(2), 159–179. Autoparametric resonance in a structure containing liquid, Part 1: two mode interaction.
15. A. Tondl 1963 *Reviews of Mechanics and Applications* **8**(4), 573–588. On the combination resonance of a nonlinear system with two degrees of freedom.

16. H. HATWALL 1982 *Journal of Sound and Vibration* **83**, 440–443. Notes on an autoparametric vibration absorber.
17. A. G. HADDOW, A. D. S. BARR and D. T. MOOK 1984 *Journal of Sound and Vibration* **97**, 451–473. Theoretical and experimental study of model interaction in a two degree of freedom structure.
18. B. BANERJEE, K. A. BAJAJ and P. DAVIES 1993 *ASME Design Technical Conferences—14th Biennial Conference on Mechanical Vibration and Noise*, **DE-54**, 127–138. Second order averaging study of an autoparametric system.
19. R. S. HAXTON and A. D. BARR 1972 *JASME Journal of Engineering for Industry* 119–125. The autoparametric vibration absorber.
20. S. R. BISHOP, D. L. XU and M. J. CLIFFORD 1996 *Proceedings of the Royal Society of London A* **452**, 1789–1806. Flexible control of the parametrically excited pendulum.
21. R.A. IBRAHIM, Y. J. YOON and M. G. EVANS 1990 *Nonlinear Dynamics* 91–116. Random excitation of nonlinear coupled oscillation.
22. O. CUVALCI and A. ERTAS 1996 *Journal of Vibration and Acoustic* **118**, 558–566. Pendulum as vibration absorber for flexible structures: experiments and theory.
23. G. MUSTAFA and A. ERTAS 1995 *ASME Journal of Dynamic Systems, Measurement, and Control*, **117**, 218–225. Experimental evidence of quasiperiodicity and its break-down in the column-pendulum oscillator.
24. A. H. NAYFEH and D. T. MOOK 1979 *Nonlinear Oscillation* New York: Wiley.
25. O. CUVALCI, A. ERTAS, I. CICEK and S. EKWARO-OSIRE *Active/Passive Vibration control and Nonlinear Dynamics of Structures* **DE-95/AMD-223**, 143–149. Vibration absorber for flexible structures: experimental study under random and sinusoidal excitations.
26. F. R. E. CROSSLEY and N. H. CONN 1953 *Journal of Applied Mechanic* 41–47. The forced oscillation of the centrifugal pendulum with wide angle.
27. J. B. HANT and J.-C. NISSEN 1982 *Journal of Sound and Vibration* **83**, 573–578. The broadband dynamic vibration absorber.
28. A. ABU-ARISH and A. H. NAYFEH 1985 *Journal of Sound and Vibration* **103**, 253–272. The response of one-degree-of-freedom systems with cubic and quadratic non-linearities to a harmonic excitation.

## NOMENCLATURE

| | |
|---|---|
| $L$ | length of the beam |
| $M$ | main mass |
| $m$ | absorber mass |
| $f$ | forcing amplitude |
| $\Omega$ | forcing frequency |
| $\omega_b$ | cantilever beam frequency with absorber locked |
| $\omega_p$ | pendulum (absorber) frequency |
| $\zeta$ | deformed elastic axis of the beam |
| $s$ | reference variable along the beam |
| $r$ | scaling factor |
| $y(s)$ | trial function belongs to a set of orthonormal functions |
| $z(t)$ | time modulations of the corresponding eigenfunction |
| $y_g(t)$ | base excitation |
| $u(\zeta, t)$ | displacement in the $x$ direction |
| $v(\zeta, t)$ | displacement in the $y$ direction |
| $\phi(\zeta, t)$ | angular displacement of the absorber |
| $M(s)$ | bending moment |
| $E$ | modules of elasticity of the beam |
| $I$ | moment of inertia of the beam |
| $(\cdot)$ | differentiation with respect to time |
| $(')$ | differentiation with respect to location |